~~RESTRICTED~~

34 P.

NACA

RESEARCH MEMORANDUM

THE AMES SUPERSONIC FREE-FLIGHT WIND TUNNEL

By Alvin Seiff, Carlton S. James, Thomas N. Canning, and Alfred G. Boissevain

Ames Aeronautical Laboratory
Moffett Field, Calif.

CLASSIFIED DOCUMENT

This material contains information affecting the National Defense of the United States within the meaning of the espionage laws, Title 18, U.S.C., Secs. 793 and 794, the transmission or revelation of which in any manner to an unauthorized person is prohibited by law.

NATIONAL ADVISORY COMMITTEE FOR AERONAUTICS

WASHINGTON
April 25, 1952

~~RESTRICTED~~
UNCLASSIFIED

NATIONAL ADVISORY COMMITTEE FOR AERONAUTICS

RESEARCH MEMORANDUM

THE AMES SUPERSONIC FREE-FLIGHT WIND TUNNEL

By Alvin Seiff, Carlton S. James, Thomas N. Canning,
and Alfred G. Boissevain

SUMMARY

The Ames supersonic free-flight wind tunnel is a new piece of equipment for aerodynamic research at high supersonic Mach numbers. It has a very wide Mach number range extending from low supersonic speeds to Mach numbers in excess of 10. The high Mach numbers are reached by firing models at high speed through the test section in a direction opposite to the wind-tunnel air stream which has a moderate supersonic Mach number. In this way, high test Reynolds numbers are attained even at the highest Mach numbers and the problem of air condensation normally encountered at Mach numbers above 5 is avoided. Aerodynamic coefficients are computed from a photographic record of the motion of the model. Methods have been developed for measuring drag, lift-curve slope, pitching-moment-curve slope, center of pressure, and damping in roll, and further extension of the use of the wind tunnel is expected.

The air stream of this wind tunnel is imperfect due mainly to a symmetrical pair of oblique shock waves which reflect down the test section. Because of the nature of the test technique, the imperfections are believed to have no serious effect on model tests.

INTRODUCTION

In many respects, the supersonic free-flight wind tunnel is closely related to the free-flight firing ranges used in ballistic research, such as those at the Ballistic Research Laboratory and the Naval Ordnance Laboratory. The two most fundamental points of difference are the use of a countercurrent air stream to produce high test Mach numbers, and the short length and small number of measuring stations to which the wind-tunnel installation is necessarily restricted.

This method of testing offers the following advantages at high supersonic speeds:

1. High Reynolds numbers
2. No air condensation problem
3. Boundary-layer temperatures comparable to those encountered in flight
4. Wide Mach number range

The main disadvantage is that aerodynamic measurements are, in general, limited to those properties which can be deduced from the recorded motion of a model in free flight. Thus far, methods have been developed for measuring drag, lift-curve slope, moment-curve slope, center of pressure, and damping in roll.

Because of the unusual nature of this equipment, and because it is proving to be very useful for certain kinds of aerodynamic research, this report has been prepared. It contains a description of the equipment and its use to obtain aerodynamic coefficients. The imperfections in the wind-tunnel air stream and their effect on model tests are also discussed.

SYMBOLS

a	horizontal component of the instantaneous acceleration of the model center of gravity normal to the tunnel center line, feet per second squared
A,B	boundary constants in roll equation
b	model span, feet
C_D	drag coefficient $\left(\frac{D}{Sq_o}\right)$
C_L	lift coefficient $\left(\frac{L}{Sq_o}\right)$
C_l	rolling-moment coefficient $\left(\frac{\text{rolling moment}}{S_w q_o b}\right)$
C_m	pitching-moment coefficient $\left(\frac{\text{pitching moment}}{Sq_o l}\right)$
C_{m_q}	damping in pitch due to rate of change of model-axis inclination relative to axes fixed in space, seconds

$C_{m_{\dot{\alpha}}}$ damping in pitch due to rate of change of model axis inclination relative to wind, seconds

C_{L_α} lift-curve slope $\left(\frac{dC_L}{d\alpha}\right)$, per radian

C_{l_ϵ} rolling-moment coefficient due to asymmetry of model

C_{l_p} damping-in-roll coefficient $\left[\frac{dC_l}{d\left(\frac{pb}{2V_o}\right)}\right]$

C_{m_α} pitching-moment-curve slope $\left(\frac{dC_m}{d\alpha}\right)$

C_1, C_2 constants used in roll calculations

D drag, pounds

E,F constants defining variation of α with time

f frequency of the pitching motion, cycles per second

H_r total pressure in wind-tunnel settling chamber, pounds per square foot

I_{xx}, I_{zz} axial and lateral moments of inertia about model center of gravity, slug feet squared

k damping constant, per second

K constant in the drag equation $\left(\frac{\rho_o S}{2m}\right)$, per foot

l model length, feet

L lift, pounds

L_ϵ, L_p rolling moment due to model asymmetry and due to rolling, respectively, foot pounds

m model mass, slugs

M_o test Mach number

M_a air stream Mach number relative to tunnel structure

p rolling velocity, radians per second

p_w free-stream static pressure from tunnel-wall measurements, pounds per square foot

q_o free-stream dynamic pressure, pounds per square foot

Q double integral with respect to time of the angle-of-attack function, seconds squared

r coordinate axis normal to tunnel axis

R Reynolds number $\left(\frac{\rho_o V_o l}{\mu_o}\right)$

s $\frac{C_2}{C_1}$

S maximum cross-sectional area of model body, square feet

S_w total included area of all wings, square feet

t time, seconds

u_a x-wise component of air-stream velocity relative to wind tunnel, feet per second

u_m x-wise component of model velocity relative to wind tunnel, feet per second

u_o x-wise component of model velocity relative to the air stream, feet per second

v_o component of resultant velocity normal to tunnel axis, feet per second

V_o resultant velocity of model relative to the air stream, feet per second

w_m y-wise component of model velocity, feet per second

x_m distance parallel to tunnel axis traveled by model relative to wind tunnel, feet

x_o distance parallel to tunnel axis traveled by model relative to air stream, feet

X_{cg}, X_{cp} distance from model nose to center of gravity and center of pressure, respectively, feet

y horizontal distance from tunnel center line, feet

α angle of attack of model relative to local flight path, radians

ϵ measure of the asymmetry of model tending to produce roll

θ angle between tunnel axis and relative wind, radians

μ_o absolute coefficient of viscosity in free stream, slugs per foot second

ρ_o free-stream air density, slugs per cubic foot

φ roll angle, radians

ω $2\pi f$

Subscripts

i refers to the initially chosen values of the constants in the roll equation

1,2,3,4 refer to times, positions, and velocities at the instants of exposure of the shadowgraphs in stations 1, 2, 3, and 4, respectively

12, 14, 23, etc. refer to intervals of time or distance between stations 1 and 2, 1 and 4, 2 and 3, etc.

EQUIPMENT AND TEST TECHNIQUES

The Wind Tunnel

The supersonic free-flight wind tunnel is a blowdown wind tunnel which utilizes the Ames 12-foot low-turbulence pressure wind tunnel as a reservoir and which exhausts to the atmosphere. Reservoir pressures up to 6 atmospheres are available. The general arrangement of the wind tunnel is illustrated in figure 1. This drawing shows plan and elevation views of the settling chamber, supersonic nozzle, test section, and diffuser. The supersonic nozzle is two-dimensional with plane side walls and rigid, symmetrical, contoured upper and lower blocks. These blocks are interchangeable, pairs being available for Mach numbers 2 and 3, but only the Mach number 2 nozzle has been used. The test section is nominally 1 foot by 2 feet in cross section and is 18 feet long. It contains windows for seven shadowgraph stations, four at 5-foot intervals along the top and three at 7.5-foot intervals along the side. Figure 2 is a photograph of the test chamber. The test section is at the left, with the black photographic plate holders of the three side stations in view. Air flow is from left to right, model flight from right to left. At the right is the control panel and a portion of the diffuser is visible above it. Two right-angle turns near the diffuser exit bar light from the tunnel interior. In addition, the interior of the tunnel is painted black to minimize light reflection.

Models and Model Launching

The research models are launched from guns located in the diffuser about 35 feet downstream of the test section (fig. 1). The guns range in bore diameter from 0.22 inch to 3 inches. At the time of this writing, the 37 millimeter size has been the largest gun used. The smaller guns are used for tests of bodies alone and the larger ones for winged models.

There are several requirements that the research models must meet which are not encountered in conventional wind tunnels. They have to be strong enough to withstand the high launching accelerations (up to 100,000 g's in extreme cases). They have to be light enough to decelerate measurably for drag determination and their moments of inertia must meet certain requirements in the case of measurement of angular motions. They must be stable so as to remain at or near the required attitude in flight. Frequently, some of the requirements conflict with others, but it has been found possible to test a wide variety of bodies and wing-body combinations. Some which are being studied are shown in figure 3(a). All three of these models can be made aerodynamically stable by proper internal design to locate the center of gravity ahead of the center of pressure. The one at the right can also be spin stabilized by launching from a rifled gun.

Launching the models without angular disturbance or damage is difficult and has required prolonged development in several cases. Elements in the development problem include: (1) building the model with the highest structural strength possible commensurate with the aerodynamic requirements of weight and stability; (2) proper choice of powder type and charge to produce lowest possible accelerating force on the model for a given velocity and given gun barrel length; (3) proper design of the plastic carrier, called a sabot, which is used as a piston to transmit the accelerating force to the model and to hold the model in proper alinement as it accelerates down the gun barrel. The key element is the sabot which must separate from the model within a few feet of the gun muzzle without imparting a large angular disturbance to the model. Several different kinds of sabots have been developed for use with different types of models. Figure 3(b) shows the disassembled sabots corresponding to the models of figure 3(a). Figure 3(c) shows the complete assemblies ready for firing. The sabot at the left separates due to aerodynamic force on the beveled leading edges of the fingers.[1] The way in which separation occurs is shown in a shadowgraph picture (fig. 4).[2] The sabot at the center of figure 3 separates because of a series of circumferential

[1]It is believed by the authors that the first extensive use of sabots of this type was at the Naval Ordnance Laboratory, White Oak, Maryland.

[2]The vertical lines in the shadowgraph are wires which the model breaks to initiate the spark. This photograph was obtained in a proof range used for launching development.

cutters rigidly mounted to the gun muzzle which act to decelerate it relative to the model. The sabot at the right is typical of those which have been used with spinning models and separates due to the shattering of the thin plastic collar by the firing impact.

The speed with which the model is launched can be varied from several hundred to several thousand feet per second by changing the type and amount of gunpowder. The wide range of launching speeds is one of the primary factors contributing to the very wide Mach number range attainable in the wind tunnel. The maximum launching speed depends on the strength of the model and sabot in resisting launching loads, or, in the case of especially rugged models, on the maximum pressure allowable in the gun. The highest velocity reached to date has been 6600 feet per second.

Range of Test Conditions

The test Mach numbers corresponding to launching velocities up to 8000 feet per second are shown in figure 5 for the three methods of operation possible with the existing equipment: no air flow through the wind tunnel, referred to as "air-off"; air flow at Mach number 2; and air flow at Mach number 3. The last two conditions are referred to as "air-on." Although Mach numbers up to 10 have been attained, no serious effort has been made to reach the maximum possible Mach number because of the need for research in the range which can now be covered.

The range of test Reynolds numbers available in the wind tunnel is shown in figure 6 for a model 4 inches long. Since the model size is considered fixed, there is no variation of Reynolds number at a given Mach number for air-off testing. Air-on, the maximum Reynolds number is three times the minimum at each Mach number. The test Reynolds number, instead of decreasing rapidly with increasing Mach number as is normal in a conventional high Mach number wind tunnel, increases linearly with the test Mach number. This is due to the linear increase of the speed of the model relative to the air while the free-stream density, viscosity, and speed of sound remain fixed. The model size selected for figure 6 is typical of the models which have been used.

Instruments

The basic wind-tunnel instruments are four shadowgraph stations which record the model position and attitude at 5-foot intervals along the test section, and a chronograph which records the time intervals between the shadowgraph pictures. These instruments are illustrated in figure 7. In addition, although not shown in figure 7, there are three shadowgraph

stations at 7.5-foot intervals in the side of the test section, used primarily to complete the three-dimensional picture of the angle of attack. Two of the side stations coincide with the first and last vertical stations. These instruments are unique in some respects and required considerable development to perfect, but only a brief description of them will be given here. A more detailed description will be found in reference 1.

Shadowgraph.- The light sources for the shadowgraphs are high intensity sparks with an effective photographic duration of about 0.3 microsecond. Light from the sparks is reflected from spherical mirrors to form parallel beams which pass up through the test section to expose photographic plates just above. The time of firing of the sparks is controlled by the model, which interrupts the light beam of a photoelectric detector just ahead of each station. This produces a signal which, after a time delay, causes the spark to discharge at the correct instant. Figure 8(a) is a shadowgraph obtained with this equipment.

Precise distance measurements must be obtained from the shadowgraph pictures. These measurements are made using an Invar scale which extends in one piece through the four shadowgraph stations, just below the photographic plates, as illustrated in figure 7. The silhouette image of a part of the scale is recorded in each shadowgraph and may be seen along the top edge of figure 8(a). To the distances obtained by measuring with reference to this scale, corrections are applied for imperfect alinement of the light beams. It has been indicated by check measurements of a known length that these corrections bring the indicated distances to within 0.0009 inch of the actual distance on the average. However, distance measurements for models moving at high speed are not this accurate because the model image is slightly blurred due to the finite duration of the spark. It has been found, however, that a given individual can locate repeatedly a reference point on the image (usually the model base) with surprising consistency. Due to this ability, and the similarity of the model images in all shadowgraphs, it has been found that an individual can make repeated distance measurements which agree among themselves, and with the measurements of other individuals to within 0.003 inch. It is believed, therefore, that the corrected distance intervals are accurate to within 0.003 inch.

Chronograph.- The time intervals between spark firings are photographically recorded on a 15-foot length of 35 mm film held at the circumference of a 5-foot-diameter film drum (fig. 7). Spot images of two kinds are distributed along this film by a high-speed rotating prism at the center of the drum. One set of spot images originates at the shadowgraph sparks where a part of the light from each spark, as it fires, is directed to the chronograph film. This is the basic time record and consists of four spots about 5 feet apart along the film. The second set of spots originates at a flashing mercury arc lamp which flashes at precisely

equal intervals. Intervals of 10, 20, 50, or 100 microseconds are used. The time between flashes is controlled by a piezo-electric crystal oscillator. These spots are about an inch apart on the film. Figure 8(b) is a small section of chronograph film with one shadowgraph spark pip at its center and several of the time-base pips on either side. The time intervals between firing of the shadowgraph sparks can be read from the film by counting the whole time-base intervals between spark pips and interpolating in the intervals where the spark pips occur. There are no known errors in this system which exceed the error of reading the film. The time-base pips are usually uniformly spaced on the film within 0.5 percent and frequently within 0.1 percent, corresponding to time-interval inequalities of 0.1 microsecond and 0.02 microsecond, respectively, for the 20-microsecond interval which is the one most frequently used. This inequality of spacing is the accumulated effect of nonuniform operation of the crystal, nonuniform response of the lamp, unequal exposure and development of pips on the film, dimensional instability of the film, and errors in reading. Although absolute accuracy is less important than relative accuracy, the crystal has been calibrated against the Bureau of Standards frequency signal and is accurate within 0.1 microsecond over a period of 1 second. The repeatability of reading the film is in the order of 0.1 microsecond and this is believed to be the accuracy of the instrument.

USE OF THE WIND TUNNEL

Although this wind tunnel was originally conceived primarily for measuring drag, it has been found possible to use it for other aerodynamic measurements as well. The development of its use is by no means complete, so that what follows here is only a tentative report of what has been done to date. More detailed discussion of the measuring procedures outlined here will be included where necessary in later reports.

Drag Measurement

Development of equation.- The equation for computing the drag coefficient is developed by writing Newton's second law for the force and acceleration components parallel to the tunnel axis.

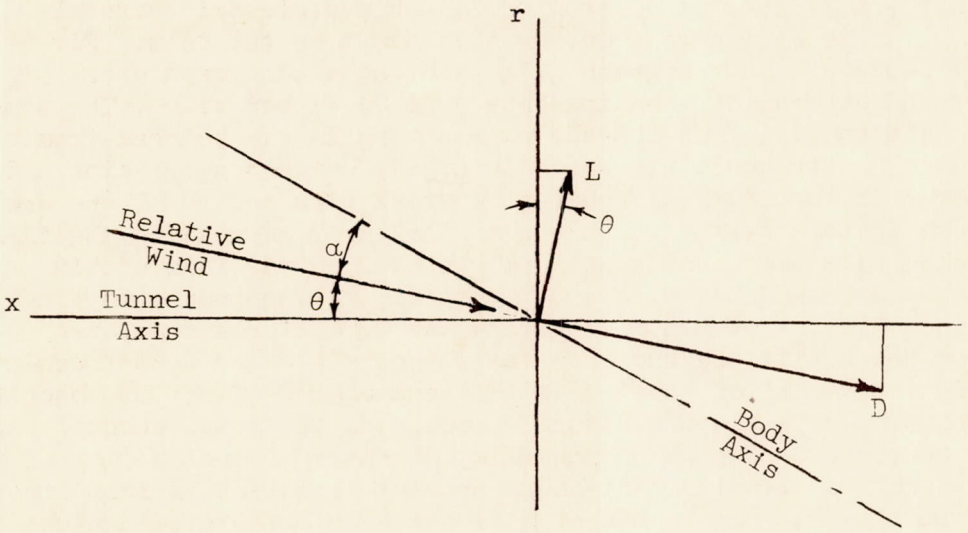

$$D \cos \theta + L \sin \theta = -m \frac{du_o}{dt} \tag{1}$$

Since θ never exceeds 2^o,

$$(C_D + C_L \theta) q_o S = -m \frac{du_o}{dt} \tag{1a}$$

Assuming that the variation of drag coefficient with angle of attack can be written

$$C_D = C_{D_{\alpha=o}} + C_{L_\alpha} \alpha^2$$

and assuming a linear lift curve

$$C_L = C_{L_\alpha} \alpha$$

equation (1a) becomes

$$(C_{D_{\alpha=o}} + C_{L_\alpha} \alpha^2 + C_{L_\alpha} \alpha\theta)\, q_o S = -m \frac{du_o}{dt} \tag{1b}$$

This development will now be restricted to those cases where the maximum value of the combination, $C_{L_\alpha} \alpha^2 + C_{L_\alpha} \alpha\theta$, is less than 0.02 $C_{D_{\alpha=o}}$ and can therefore be neglected. With this restriction, equation (1b) becomes

$$C_D q_o S = -m \frac{du_o}{dt} \tag{1c}$$

The approximate expression for dynamic pressure, $\frac{1}{2}\rho_o u_o^2$, differs by less than 0.04 percent from the exact expression, $\frac{1}{2}\rho_o V_o^2$, because $v_o < 0.02u_o$, and will be used here

$$C_D \frac{1}{2} \rho_o u_o^2 S = -m \frac{du_o}{dt} \tag{1d}$$

$$C_D \frac{\rho_o S}{2m} dt = - \frac{du_o}{u_o^2} \tag{1e}$$

$$KC_D dt = - \frac{du_o}{u_o^2} \tag{1f}$$

Using the lower limits, $x_o = 0$ and $u_o = u_{o_1}$ when $t = 0$, two integrations of equation (1f) give the following logarithmic expression:

$$KC_D x_o = \ln(KC_D u_{o_1} t + 1) \tag{2}$$

The unknown C_D occurs both inside and outside the logarithm and cannot be calculated except by trial and error. Expanding the logarithm in series reduces the difficulty.

$$KC_D x_o = KC_D u_{o_1} t - \frac{1}{2}(KC_D u_{o_1} t)^2 + \frac{1}{3}(KC_D u_{o_1} t)^3 \ldots + \frac{(-1)^{n-1}}{n}(KC_D u_{o_1} t)^n \tag{3}$$

Noting that

$$x_o = x_m + u_a t, \text{ and } u_{o_1} = u_{m_1} + u_a$$

and dividing through by KC_D yields

$$x_m = u_{m_1} t - \frac{1}{2}(KC_D)(u_{o_1} t)^2 + \frac{1}{3}(KC_D)^2(u_{o_1} t)^3 \ldots + \frac{1}{n}(-KC_D)^{n-1}(u_{o_1} t)^n \tag{3a}$$

Equation (3a) is the working equation for the calculation of drag coefficient. The terms

$$x_m = u_{m_1} t - \frac{1}{2}(KC_D u_{o_1}^2) t^2$$

are the equation of uniformly decelerated motion, since $KC_D u_{o_1}^2$ is the value of the deceleration at $t = 0$. The additional terms are due to the decrease in dynamic pressure with time as the model decelerates. In practice, the series converges rapidly. Terms in powers of t greater than 4 are rarely significant.

Use of equation.- The quantities x_m, t, and K in equation (3a) are obtained from the time-distance record, from model measurements, and from the air-stream calibration. Two quantities, u_{m_1} and C_D are unknown.

Two numerically independent equations can be written from (3a) using x_m and t data from three stations. These two equations are solved simultaneously for C_D by an iterative procedure.

Since only three stations are required to compute C_D and four are available, the data from a single model launching are redundant and can be used to compute four values of drag coefficient. The average of the four is assumed to be the best value for the round. A least-squares procedure could be used, but would complicate the data reduction without significantly improving the results since the scatter of the four values of C_D, typically, is ±2 percent.

Accuracy.- The accuracy with which drag coefficient can be measured depends on the drag coefficient and mass per unit frontal area of the model. The deceleration must be sufficient to cause measurable difference between the actual motion and an undecelerated motion. In particular, the quantity $(u_{m_1} t_{14} - x_{14})$, hereinafter referred to as the distance decrement, must be larger than 0.5 inch if the experimental scatter is to be less than ±2 percent. This quantity is affected by the drag coefficient, the body fineness ratio, the scale of the model, and the materials and methods of model construction, and its importance must be fully appreciated in planning tests since some models are unsatisfactory or marginal in this respect. In other cases, there is no difficulty in obtaining the required distance decrement. The range of values of distance decrement encountered thus far has been from 0.3 inch to 10 inches.

A typical set of drag measurements is presented in figure 9 where drag coefficient is plotted as a function of Mach number for a 60° cone cylinder with a cylinder fineness ratio of 1.2. The distance decrements in this figure ranged from 1.8 to 4.5 inches. The average scatter of the four results obtained with an individual model was ±1.4 percent. The mean deviation of the experimental points from the faired curve is 1.2 percent.

Measurements of Lift-Curve Slope, Pitching-Moment-Curve Slope, and Center of Pressure

Lift-curve slope.- A method which can be used to obtain C_{L_α} involves measuring the curvature of the flight path caused by lift of a model oscillating in pitch. The model is designed to execute between 1/2 and 1-1/4 pitching oscillations in the test section and is disturbed at launching so as to oscillate with an amplitude of about 5° in the horizontal plane. Small oscillations in the vertical plane also occur due to accidental disturbances. The complete motion in three dimensions cannot be studied because of inadequate data in the vertical plane. Instead,

the projection of the motion in the horizontal plane is used assuming that the interaction between pitch and yaw is small. The angle of attack of the model and the lateral position of its center of gravity are carefully measured from the shadowgraph pictures to provide the basic data.

Using Newton's second law of motion, the instantaneous acceleration of the center of gravity of the model normal to the tunnel axis may be written as follows:

$$a = \frac{d^2y}{dt^2} = \frac{C_{L_\alpha} \alpha q_o S}{m} \tag{4}$$

This equation neglects the contribution of the drag force to the lateral acceleration (see diagram on p. 10). The latter contribution is usually negligible, but need not be so in every case, so care must be exercised to see if this omission is permissible. The angle of attack in this expression varies with time, and the assumption is made that the lift force varies linearly with the angle of attack.

An equation describing the variation of angle of attack with time can be written using the angle-of-attack measurements from the shadowgraph pictures and two assumptions which define the form of the motion. The assumptions are that the restoring moment in pitch is directly proportional to the angle of attack and that the damping moment in pitch is directly proportional to the pitching rate. These assumptions lead to the following differential equation:

$$I_{zz} \frac{d^2\alpha}{dt^2} + (C_{m_{\dot{\alpha}}} + C_{m_q}) q_o S l \frac{d\alpha}{dt} + C_{m_\alpha} q_o S l \alpha = 0 \tag{5}$$

The solution of this equation is a damped sine wave given by:

$$\alpha = e^{-kt}(E \cos \omega t - F \sin \omega t) \tag{6}$$

Equation (6) is fitted to the observed variation of α with respect to time by a least-squares procedure described in reference 2. In this way, the four unknowns, ω, k, E, and F, are evaluated. The complete set of four shadowgraphs is required to determine the sine wave so the method of least squares is not strictly required but is used as a convenient and systematic method.

Combining equations (4) and (6) gives the instantaneous lateral acceleration as a function of time:

$$\frac{d^2y}{dt^2} = \frac{dw_m}{dt} = \frac{C_{L_\alpha} q_o S}{m} e^{-kt}(E \cos \omega t - F \sin \omega t) \tag{7}$$

Integrating with respect to t gives the following equation for lateral velocity as a function of time:

$$w_m = \frac{dy}{dt} = w_{m_1} + \frac{C_{L_\alpha} q_o S}{m} \int_{t_1}^{t} e^{-kt}(E \cos \omega t - F \sin \omega t)dt \qquad (8)$$

where w_{m_1} is the lateral velocity at the first station. A second integration gives the equation of lateral displacement. This time the integrals are evaluated between limits corresponding to the times and lateral positions in two shadowgraph stations.

$$y_2 = y_1 + w_{m_1}(t_2 - t_1) + \frac{C_{L_\alpha} q_o S}{m} \int_{t_1}^{t_2}\int_{t_1}^{t} e^{-kt}(E \cos \omega t - F \sin \omega t)dt\, dt \qquad (9a)$$

The double integral on the right can be evaluated since both the integrand and the limits are known. For brevity, it will be designated Q_{12}.

$$y_2 = y_1 + w_{m_1}(t_2 - t_1) + \frac{C_{L_\alpha} q_o S}{m} Q_{12} \qquad (9b)$$

In this equation, the unknowns are C_{L_α} and w_{m_1}. The quantity w_{m_1} can be eliminated by using data from a third station.

$$y_3 = y_1 + w_{m_1}(t_3 - t_1) + \frac{C_{L_\alpha} q_o S}{m} Q_{13} \qquad (9c)$$

Solving equations (9b) and (9c) simultaneously yields the following expression for C_{L_α}:

$$C_{L_\alpha} = \frac{m}{S q_o} \frac{y_{12} - y_{13}(t_{12}/t_{13})}{Q_{12} - Q_{13}(t_{12}/t_{13})} \qquad (10)$$

As was the case with drag coefficient, four independent values of C_{L_α} can be obtained from a four-station run.

The primary requirement for a good test run is that the curvature of the flight path in the test section be large enough to be measured accurately. Early results have indicated that if a straight line is drawn between two measured positions of the model, points 1 and 3, the lift-curve slope may be obtained within ±7 percent if point 2 falls at least 0.20 inch off the line. It is expected that future improvements in experimental technique will reduce this requirement.

Pitching-moment-curve slope and center of pressure.- The least-squares fit to the variation of angle of attack with time establishes the pitching frequency, ω. This makes it possible to obtain the pitching-moment-curve slope about the center of gravity from the relation

$$f = \frac{1}{2\pi}\sqrt{\frac{C_{m_\alpha} S q_o l}{I_{zz}}} \tag{11}$$

The scatter in repeated determinations of the frequency is about ±5 percent. This results in a scatter of about ±10 percent in C_{m_α}.

The center of pressure can be obtained from the lift and pitching-moment results using the relation:

$$\left(\frac{X_{cp} - X_{cg}}{l}\right) C_{L_\alpha} = C_{m_\alpha} \tag{12}$$

The center of pressure can be repeatedly measured in this way with a scatter of about ±2 percent of the body length. The percentage errors in the margin of stability, $X_{cp} - X_{cg}$, which is the quantity directly given by equation (12), are consistent with the percentage errors in lift and pitching moment. However, the margin of stability is small compared to the body length (from 0.05 l to 0.15 l), so the error in X_{cp} expressed as a fraction of the body length is much smaller than the errors in lift and pitching moment.

Damping in Roll

The damping in roll of tail-body combinations can be measured by launching the models from rifled guns and recording photographically the roll angle as a function of time as the model passes through the test section. A high-speed motion picture camera is used to photograph the tail-on view of the model. Depending on the velocity of the model, from 8 to 50 photographs can be obtained of the model while it is in the test section. Roll angles are accurately measured from the photographs on the film strip. These are linked by a time reference which is printed on the margin of the film by a flashing argon lamp as the photographs are being taken. To these data is fitted an equation defining the pure rolling motion of an axially symmetric missile. The method used is essentially that of Bolz and Nicolaides, reported in reference 3. The primary difference between the derivation of reference 3 and that which follows here is in the choice of the independent variable. Because of the method of photographing the motion, it was found desirable to choose time as the independent variable rather than distance.

The equation of motion of an axially symmetric missile in pure rolling flight (single degree of freedom) is

$$I_{xx} \frac{d^2\varphi}{dt^2} = L_\epsilon + L_p \tag{13}$$

in which L_ϵ and L_p are the rolling moments acting on the missile due to out-of-trim fin alinement and rolling velocity, $d\varphi/dt$, respectively. Equation (13) can be rewritten in the form

$$\frac{d^2\varphi}{dt^2} + C_1\frac{d\varphi}{dt} - C_2 = 0 \tag{14}$$

where

$$C_1 = -\frac{\rho_o S_w b^2 V_o}{4I_{xx}} C_{l_p}$$

and

$$C_2 = \frac{\epsilon q_o S_w b}{I_{xx}} C_{l_\epsilon}$$

where C_1 and C_2 are assumed constant. The general solution of equation (14) is

$$\varphi = B + st + Ae^{-C_1 t} \tag{15}$$

where $s = C_2/C_1$, the steady-state rolling velocity.

The experimental procedure is to fit equation (15) to the measured variation of φ with time with the objective of evaluating C_1. The measurements of roll position are not highly precise, but the data are redundant so that a statistical fit is the best approach to a reliable answer. In order to make possible a least-squares fit to the data, it is necessary to linearize equation (15). Initial values are chosen, by the method described in reference 3, for the constants in equation (15) which is then expanded in a Taylor series about these initial values.

$$\varphi = B_i + s_i t + A_i e^{-C_{1i} t} + \Delta B + t\Delta s + e^{-C_{1i} t}\Delta A - tA_i e^{-C_{1i} t}\Delta C_1 -$$

$$t e^{-C_{1i} t}\Delta C_1 \Delta A + \frac{1}{2} t^2 A_1 e^{-C_{1i} t}(\Delta C_1)^2 + \ldots \tag{16}$$

in which ΔB, Δs, ΔA, and ΔC_1 are corrections to the assumed values of the constants. All terms in ΔC_1 and ΔA of order two or greater may be neglected if ΔC_1 and ΔA are small. Then

$$\varphi - \varphi_i = \Delta B + t\Delta s + e^{-C_{1i} t}\Delta A - tA_i e^{-C_{1i} t}\Delta C_1 \tag{17}$$

where

$$\varphi_i = B_i + s_i t + A_i e^{-C_{1i} t}$$

the roll angle calculated from initial values of the constants of equation (15). Equation (17) is then used to obtain the corrections to these initial values by the method of least squares using the measured values of roll angle. The iterative solutions of equation (17) are convergent if initial values of the constants of equation (15) are chosen with reasonable care. Three or four iterations are usually sufficient to reduce the corrections to negligible magnitude.

A few measurements of C_{l_p} by this method have been obtained for the air-off condition of the wind tunnel. Four measurements near the same Mach number show a scatter of ±3 percent. The damping derivatives obtained show good agreement with linearized theory which is the expected result for the low supersonic Mach number at which the test was run.

IMPERFECTIONS IN THE WIND-TUNNEL AIR STREAM AND THEIR EFFECT ON MODEL TESTS

An extensive air-stream survey in which total head, static pressure, and stream angle were measured showed the main source of air-stream imperfections to be a pair of oblique shock waves which originate at the inflection point of the nozzle and reflect down the channel as shown in figure 10. It is coincidental that the waves reflect from the smooth joint between the nozzle blocks and the test-section walls. With the original position of the upper and lower walls (which were slightly divergent to compensate for boundary-layer growth), the wave pattern caused the Mach number to decrease stepwise along the length of the test section. Because of the desirability of maintaining a constant average Mach number, the upper and lower walls of the test section were diverged farther so that the flow expanded steadily to compensate for the stepwise compression at the shocks. The resulting axial Mach number distribution is shown in figure 11.

In some applications, the existence of oblique shock waves comparable to those occurring here would seriously affect the accuracy of the aerodynamic testing. In the present case, the indication is that the oblique waves, while undesirable, do not introduce large errors in the test results. This indication is developed in the following paragraphs where four effects of the wave system on model tests are discussed.

Test Mach number.- As a consequence of the periodic variations in air-stream velocity and speed of sound, the test Mach number varies periodically as the model advances through the test section. The magnitude of the variation depends on the test Mach number and ranges from ±0.05 at a Mach number of 4 to ±0.10 at a Mach number of 10.

Dynamic pressure.- The shock-wave system affects the test dynamic pressure since both the density and velocity of the air stream are affected. The magnitude of the variation in dynamic pressure ranges from ±2.5 percent at a Mach number of 4 to ±3.2 percent at a Mach number of 10. The pattern of variation at a test Mach number of 4 is shown in figure 12.

In computing the aerodynamic coefficients from the data, the dynamic pressure is assumed to be constant at its mean value. In the case of drag measurement, this assumption introduces scatter in the results because the mean dynamic pressures in the three shadowgraph intervals are not exactly equal. The scatter from this cause has been estimated at less than 0.5 percent. In the case of pitching or rolling motions, the unsteadiness of the dynamic pressure slightly distorts the motions and causes an apparent scatter of the measurements of angular position about the idealized curve.

Static pressure.- A large static-pressure variation in the stream direction exists due to the shock-wave system. The pressure distribution along the upper and lower walls is plotted in figure 13. The maximum variation is ±4.5 percent from the mean value. In spite of this large variation, the errors which result are believed to be small for three reasons:

1. The pressure difference fore and aft on the model is not the full peak-to-peak value but a small fraction of this amount because the model is short compared to the cycle.

2. The axial force caused by this pressure difference is negligibly small compared to the drag because the test dynamic pressures are very large. The quantity $\frac{\Delta p_o}{q_o}$ ranges from 0.0083 at $M_o = 4$ to 0.0013 at $M_o = 10$.

3. The effect of the pressure gradient on model position is compensating within any complete cycle because the gradient alternately adds to and subtracts from the drag.

Stream angle.- Stream angularity up to 1° in a vertical plane and up to 0.4° in a horizontal plane was measured within the air stream. The stream-angle variation relative to the model is reduced 50 percent or more from its value relative to the tunnel because the upstream velocity of the model adds vectorially to the velocity of the air stream. Therefore, to a model proceeding upstream along the tunnel axis, the variation in stream direction is less than $\pm 0.5^\circ$ in a vertical plane and $\pm 0.2^\circ$ in a horizontal plane. The effect on the drag of angles of attack of this magnitude is small. The effect of the stream-angle variation on pitching motions is believed to be small for the following reasons:

1. The pitching motions are studied in the horizontal plane where the stream angularity is least.

2. The amplitude of the stream-angle variation is small compared to the amplitude of the pitching oscillation.

3. The frequency of the stream-angle variation is about five times the designed frequency of oscillation of the models so the response of the models to the impressed variation is very weak.

CONCLUDING REMARKS

The operation and usefulness of the Ames supersonic free-flight wind tunnel as a research facility has been described. The aerodynamic properties which may be studied in this wind tunnel include:

1. Drag
2. Lift-curve slope
3. Pitching-moment-curve slope
4. Center of pressure
5. Damping in roll

These measurements can be made over a wide range of Mach numbers and Reynolds numbers at temperatures approaching actual flight conditions for missiles. Techniques are being developed to measure aerodynamic properties other than those enumerated here.

Ames Aeronautical Laboratory,
National Advisory Committee for Aeronautics,
Moffett Field, Calif.

REFERENCES

1. Briggs, Robert O., Kerwin, William J., and Schmidt, Stanley F.: Instrumentation of the Ames Supersonic Free-Flight Wind Tunnel. NACA RM A52A18, 1952.

2. Shinbrot, Marvin: A Least-Squares Curve-Fitting Method With Applications to the Calculation of Stability Coefficients From Transient-Response Data. NACA TN 2341, 1951.

3. Bolz, Ray E., and Nicolaides, John D.: A Method of Determining Some Aerodynamic Coefficients from Supersonic Free Flight Tests of a Rolling Missile. Rept. 711, Aberdeen Ballistic Research Laboratories, Dec. 1949.

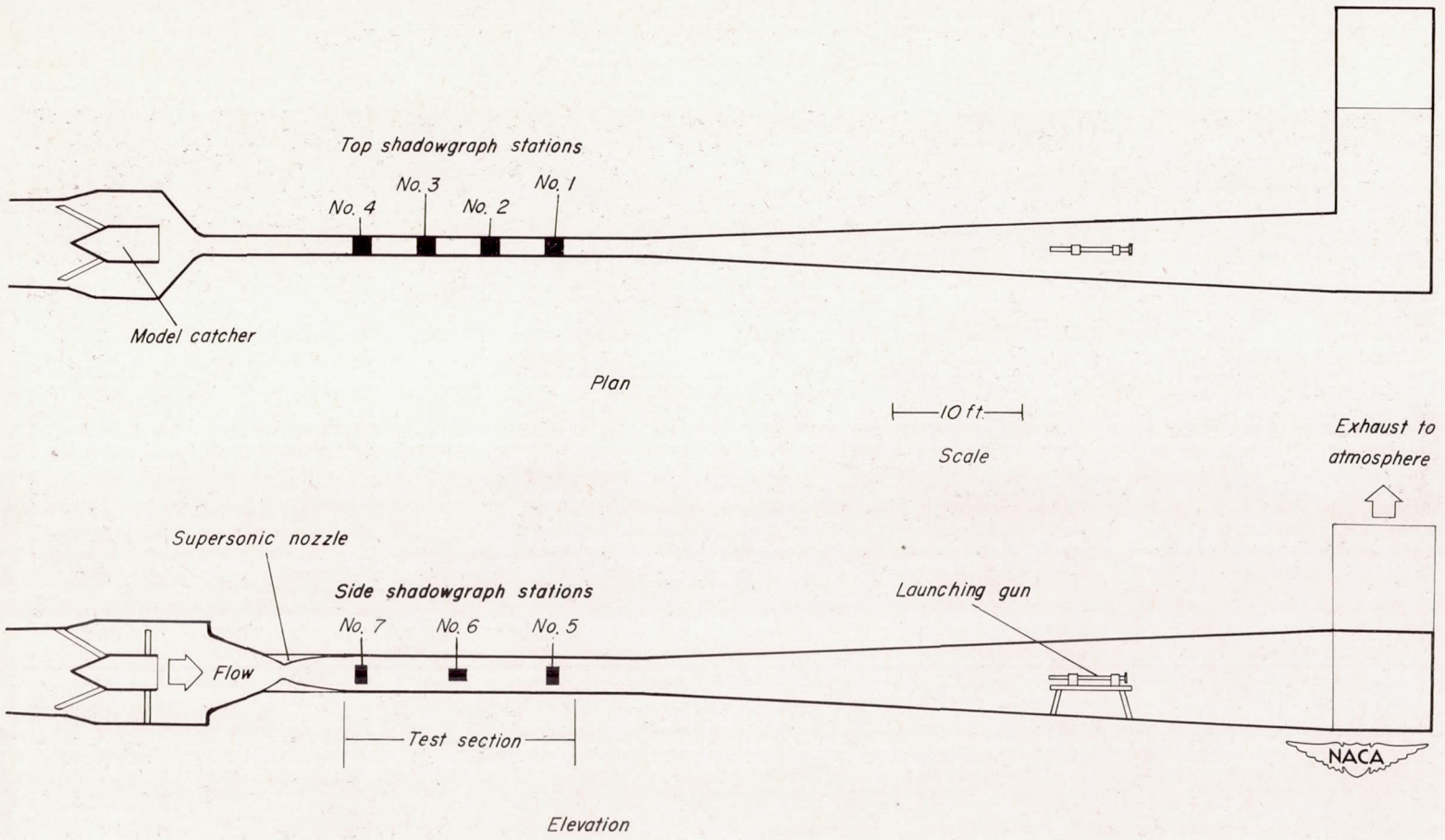

Figure 1. – The Ames Supersonic Free - Flight Wind Tunnel - general arrangement.

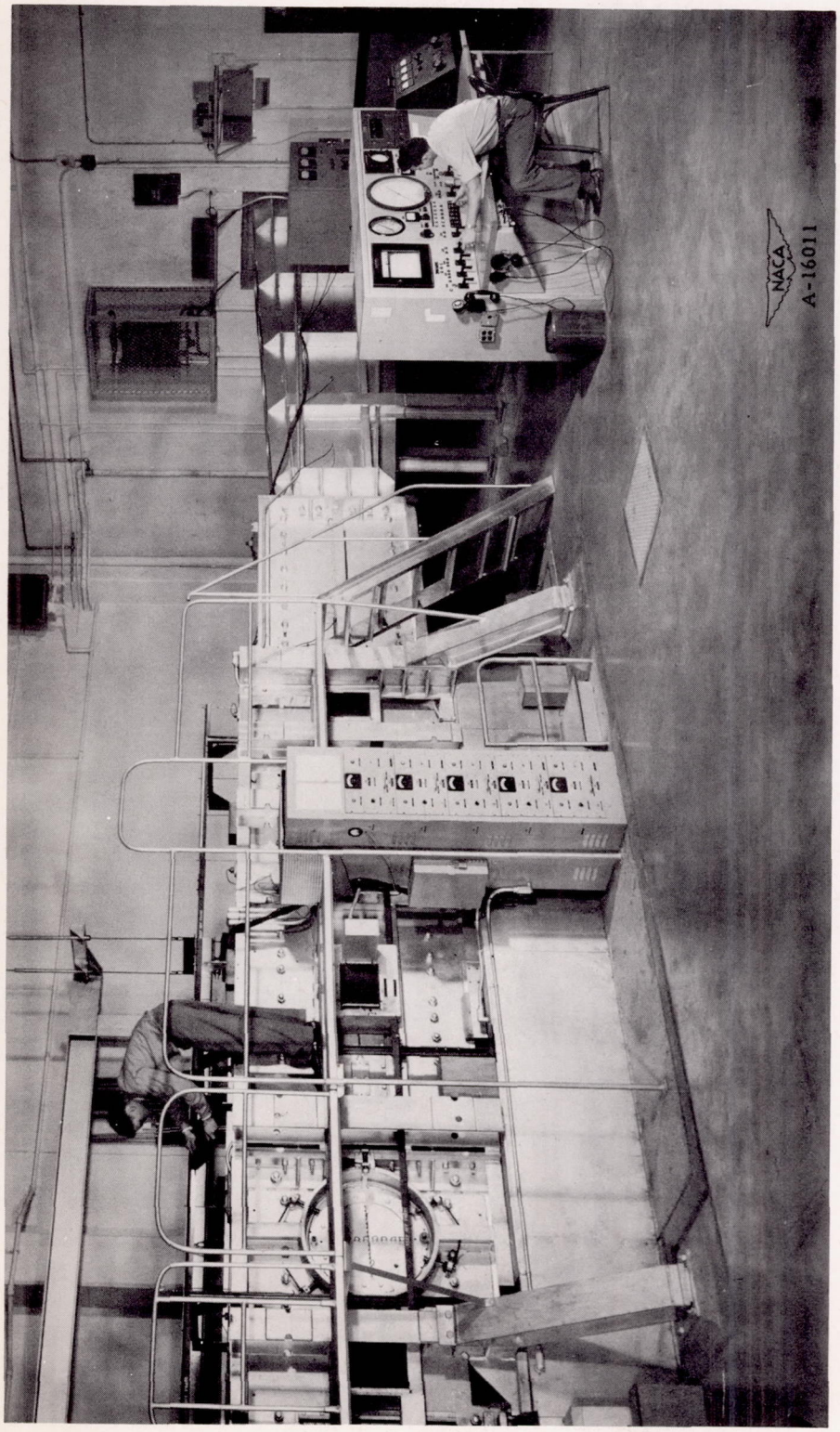

Figure 2.- Photograph of test section and control panel.

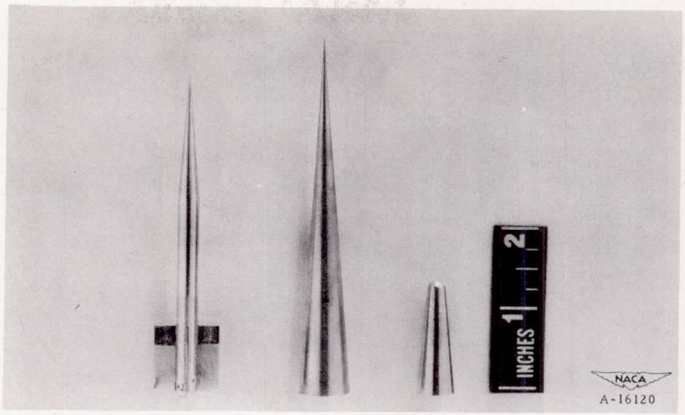

(a) Models.

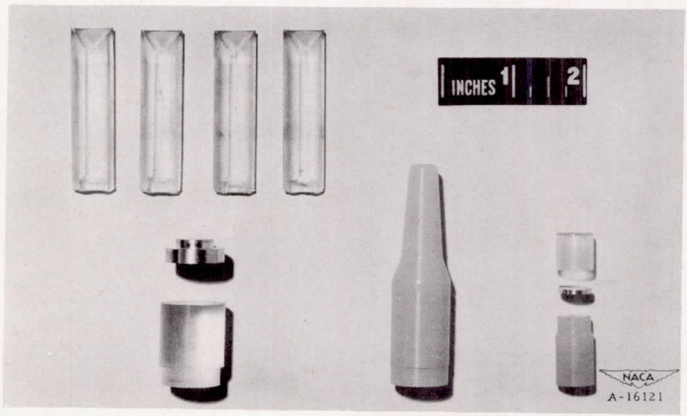

(b) Sabots.

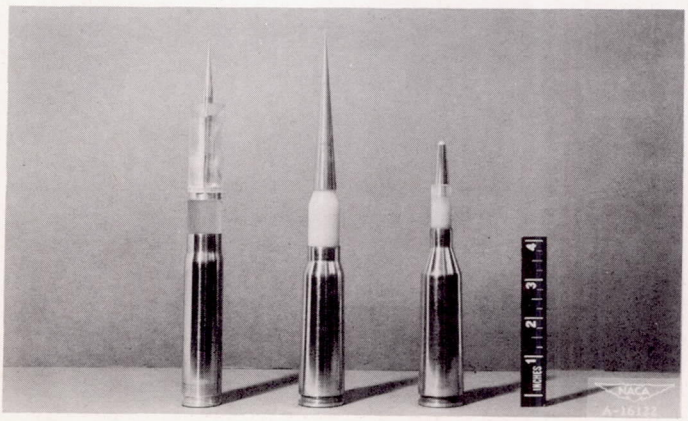

(c) Assemblies ready for launching.

Figure 3.- Models and sabots.

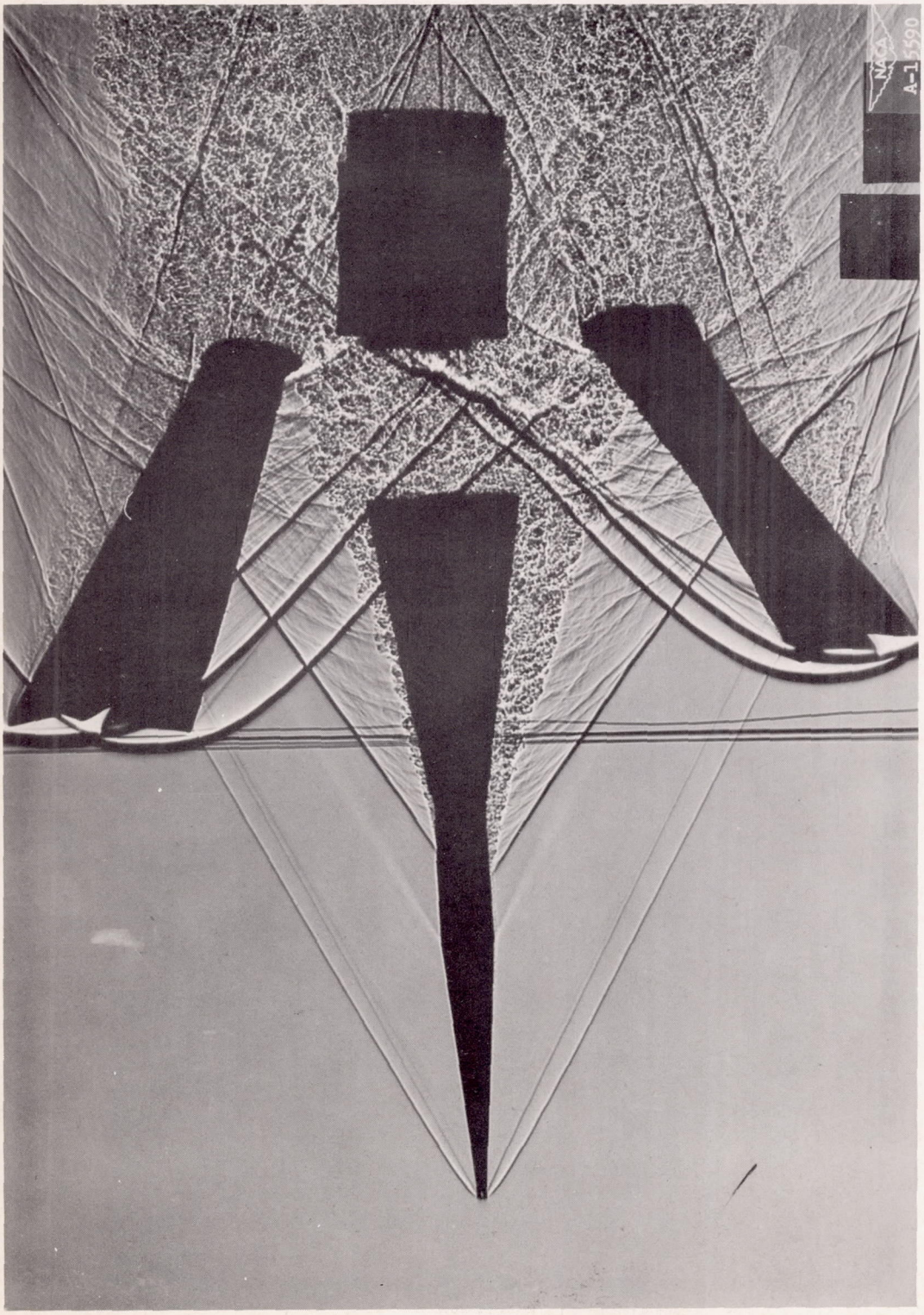

Figure 4.- Shadowgraph of the separation of a finger-type sabot.

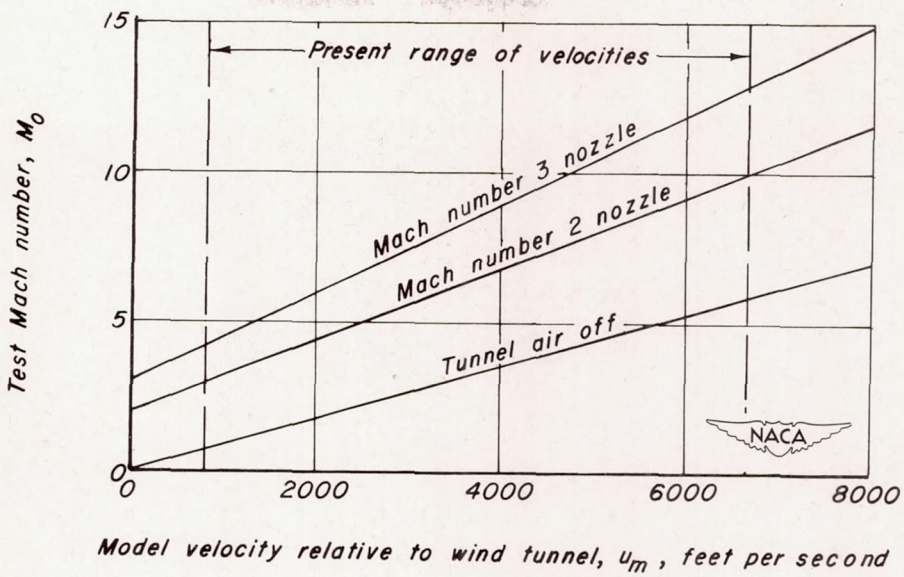

Figure 5.- Range of test Mach numbers.

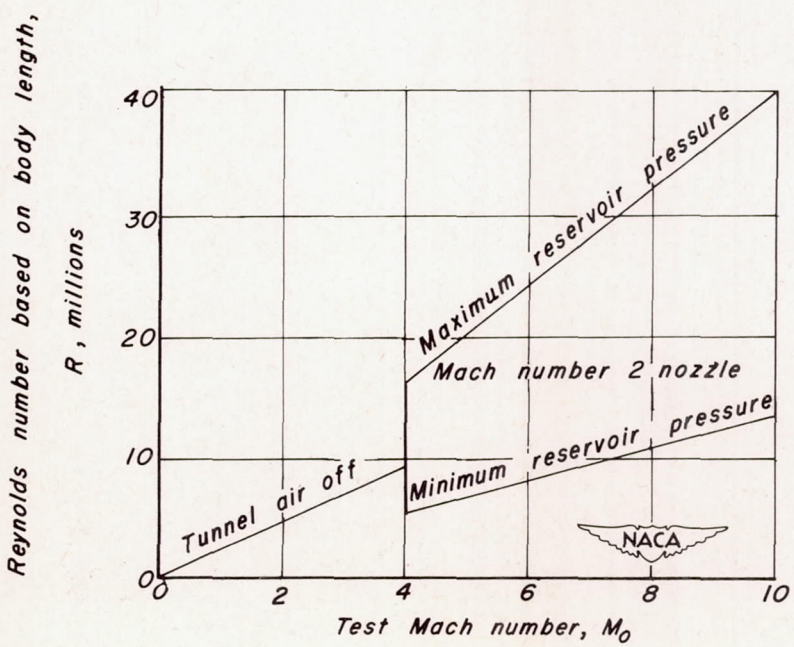

Figure 6.- Range of test Reynolds numbers for a model 4 inches long.

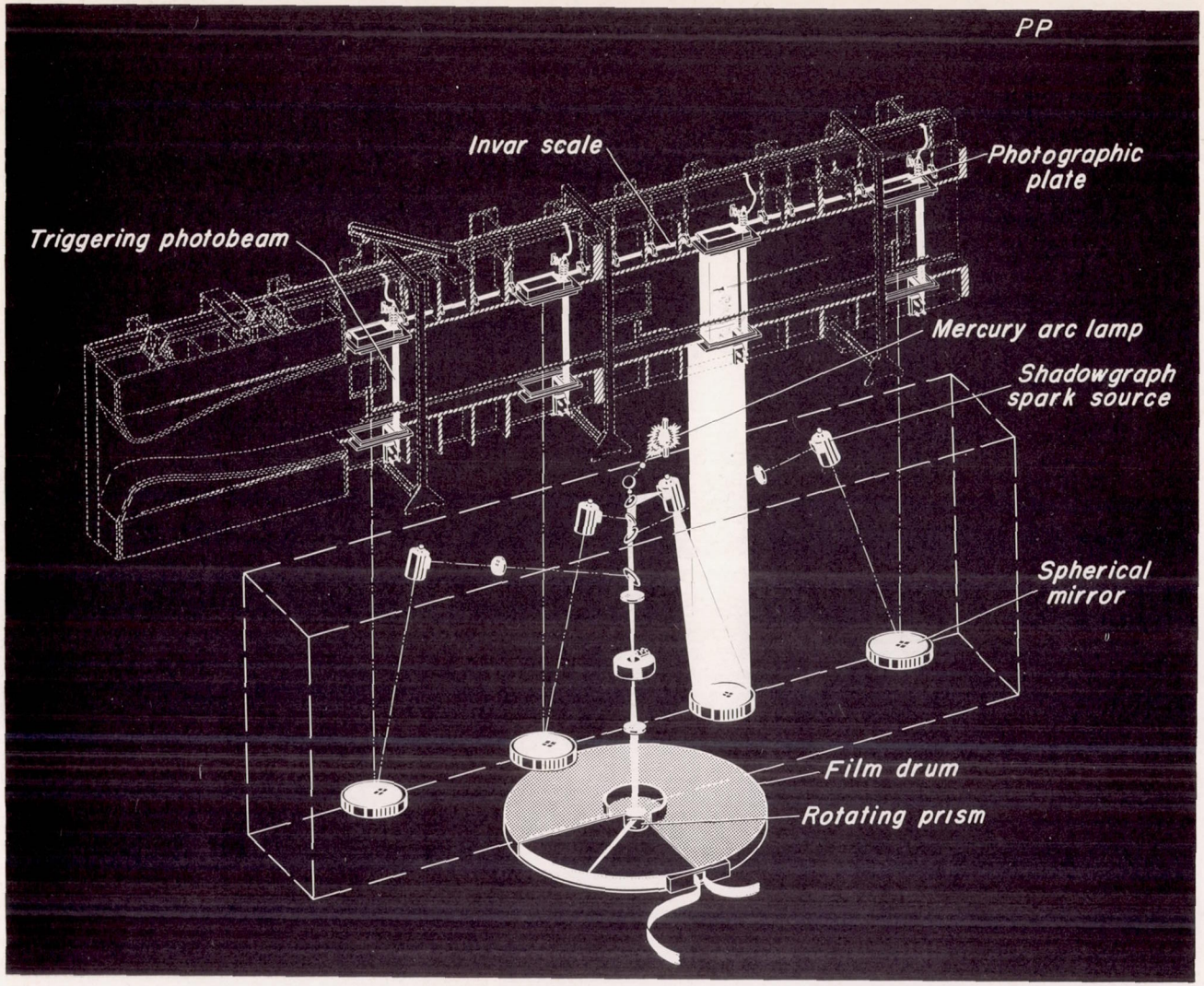

Figure 7.- Schematic drawing of the time-distance instruments.

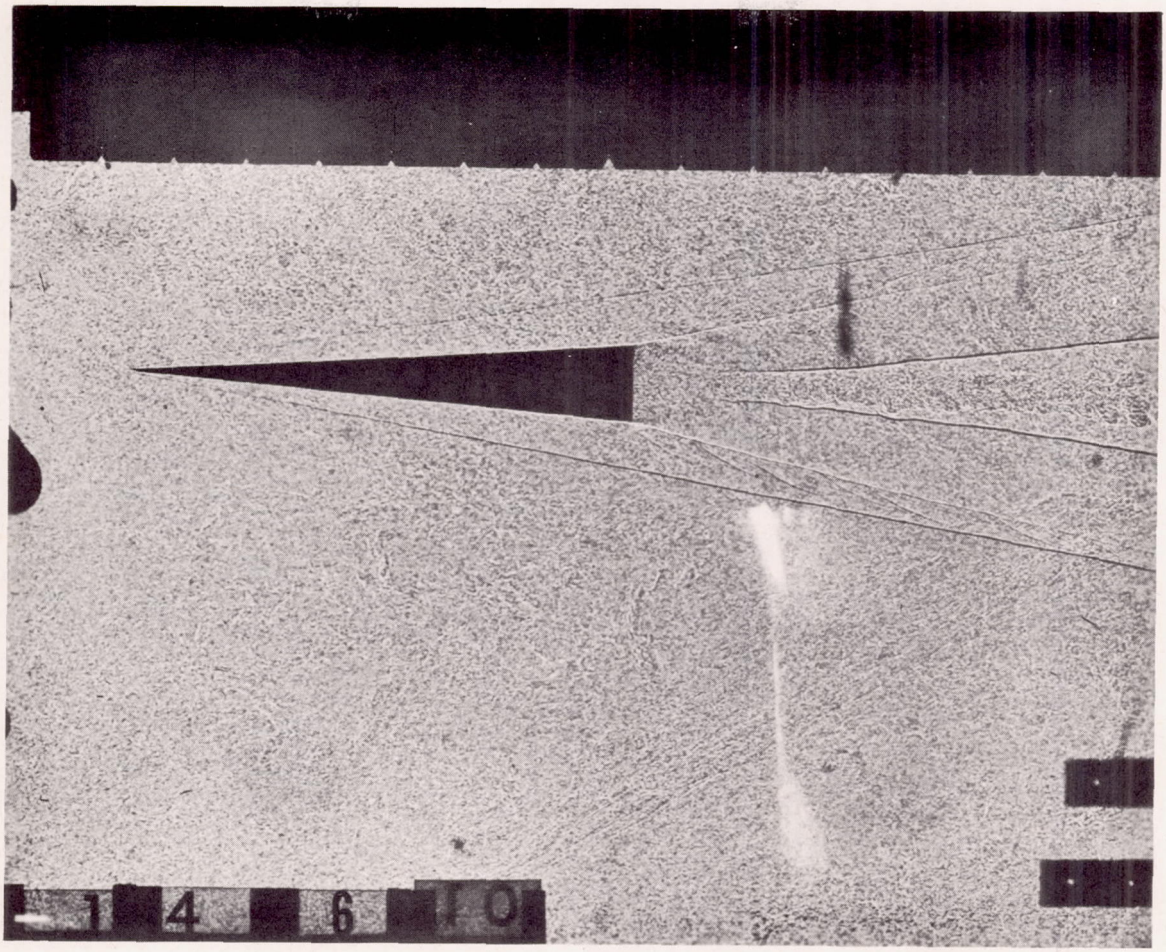

(a) Shadowgraph.

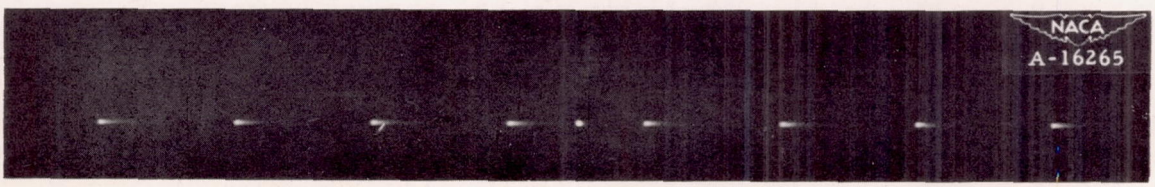

(b) Section of chronograph film.

Figure 8.- Samples of the time-distance record.

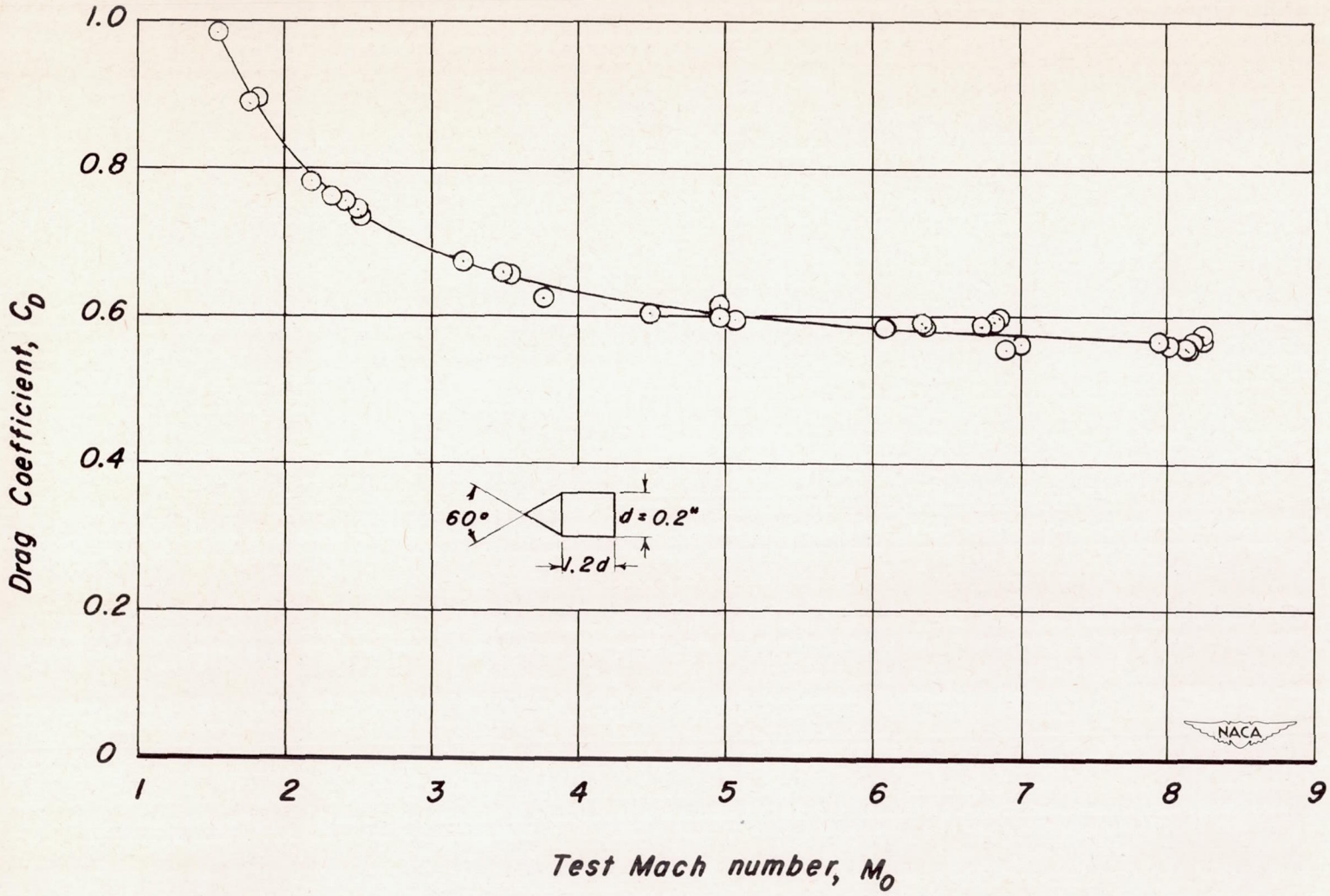

Figure 9. – Measurements of the drag coefficient of a 60° cone cylinder.

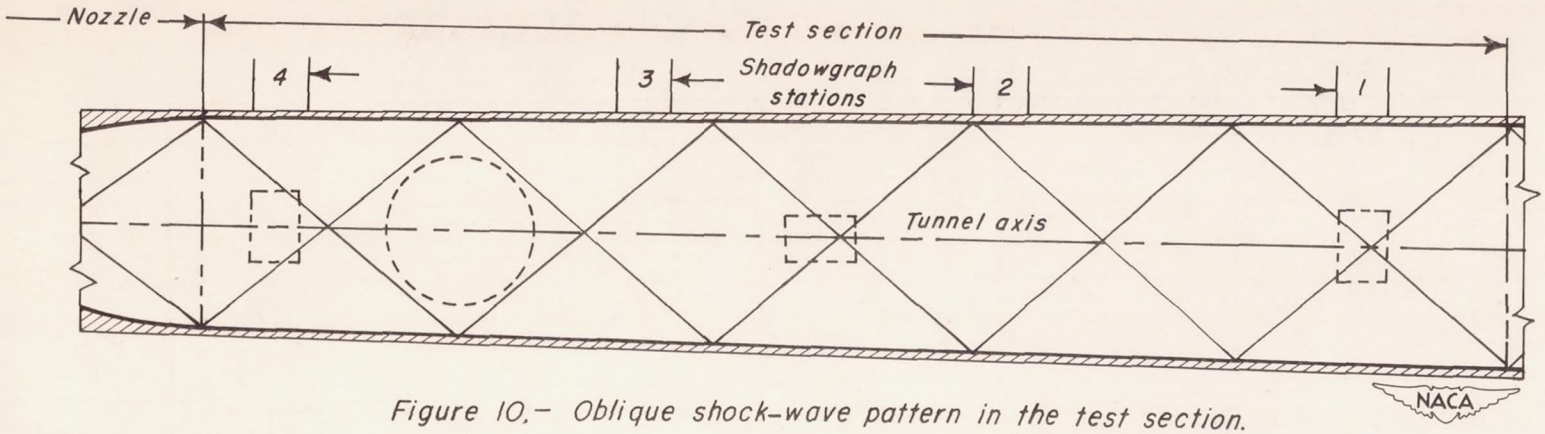

Figure 10.– Oblique shock-wave pattern in the test section.

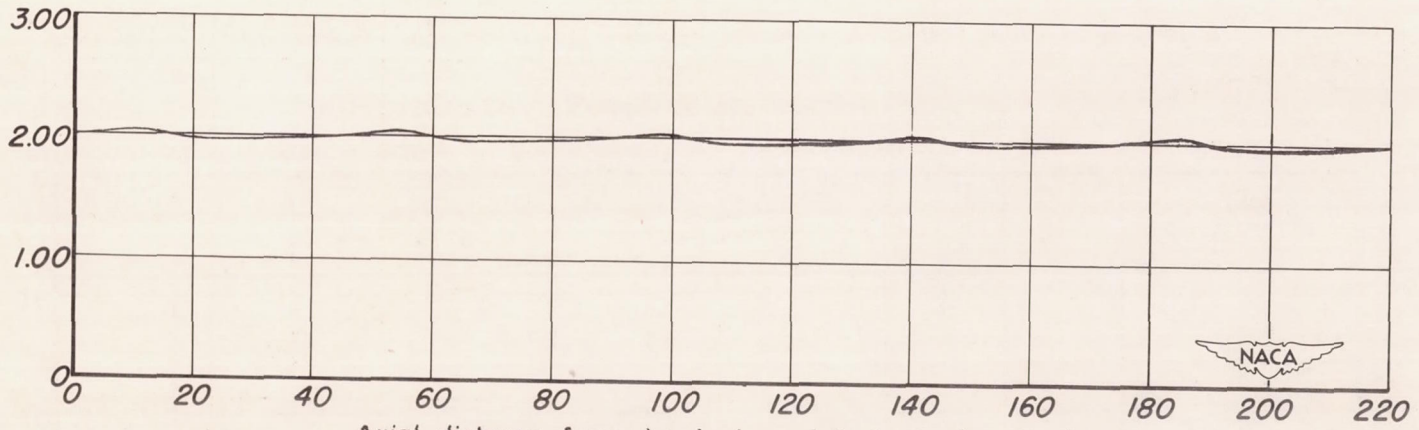

Axial distance from beginning of test section, (inches)

Figure 11.– Axial variation of air-stream Mach number.

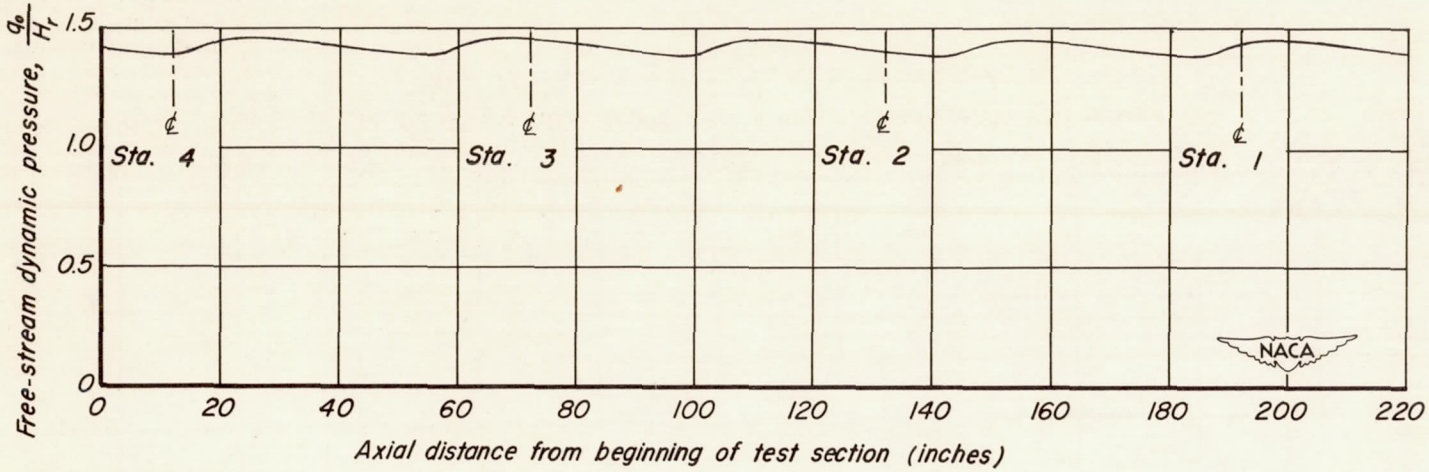

Figure 12.- Axial variation of free-stream dynamic pressure for a test Mach number of 4.

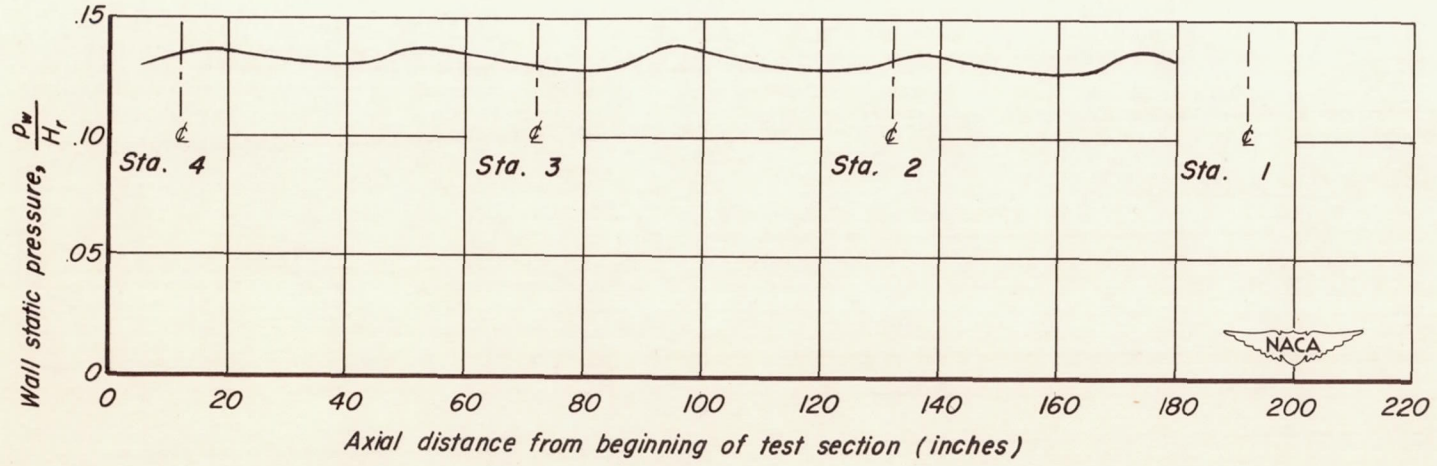

Figure 13.- Longitudinal variation of wall static pressure.

NACA-Langley - 4-25-52 - 375